

PCCP

Accepted Manuscript



This is an *Accepted Manuscript*, which has been through the Royal Society of Chemistry peer review process and has been accepted for publication.

Accepted Manuscripts are published online shortly after acceptance, before technical editing, formatting and proof reading. Using this free service, authors can make their results available to the community, in citable form, before we publish the edited article. We will replace this *Accepted Manuscript* with the edited and formatted *Advance Article* as soon as it is available.

You can find more information about *Accepted Manuscripts* in the [Information for Authors](#).

Please note that technical editing may introduce minor changes to the text and/or graphics, which may alter content. The journal's standard [Terms & Conditions](#) and the [Ethical guidelines](#) still apply. In no event shall the Royal Society of Chemistry be held responsible for any errors or omissions in this *Accepted Manuscript* or any consequences arising from the use of any information it contains.

***Ab initio* quantum dynamical analysis of ultrafast nonradiative transitions
via conical intersections in pyrazine**

Manabu Kanno,^{*a} Yuta Ito,^b Noriyuki Shimakura,^{†b} Shiro Koseki,^c Hirohiko Kono^a
and Yuichi Fujimura^{ad}

^a *Department of Chemistry, Graduate School of Science, Tohoku University,
Sendai 980-8578, Japan*

^b *Department of Chemistry, Niigata University, Ikarashi Nino-cho 8050, Niigata 950-2181, Japan*

^c *Department of Chemistry, Graduate School of Science, and Research Institute for Molecular
Electronic Devices (RIMED), Osaka Prefecture University, 1-1 Gakuen-cho, Naka-ku,
Sakai 599-8531, Japan*

^d *Department of Applied Chemistry, Institute of Molecular Science, and Center for Interdisciplinary
Molecular Science, National Chiao-Tung University, Hsin-Chu 300, Taiwan*

*E-mail: kanno@m.tohoku.ac.jp

†E-mail: shima@emeritus.niigata-u.ac.jp

Abstract

We theoretically investigated the mechanism of ultrafast nonradiative transition through conical intersections in photoexcited pyrazine by *ab initio* quantum dynamical calculations. This work was motivated by the recent theoretical and experimental studies that presented conflicting results: The former is the on-the-fly semiclassical surface hopping calculation combined with the time-dependent density functional theory, which showed that nonadiabatic transitions from the optically bright S_2 ($^1B_{2u}, \pi\pi^*$) state to the optically dark S_3 ($^1A_u, n\pi^*$) and S_4 ($^1B_{2g}, n\pi^*$) states take place predominantly at the initial stage of electronic relaxation [U. Werner *et al.*, *Chem. Phys.*, 2008, **349**, 319]; the latter is the pump-probe photoelectron spectroscopic measurement which reported the S_2 lifetime (22 ± 3 fs) of nonradiative decay to the almost dark S_1 ($^1B_{3u}, n\pi^*$) state [Y.-I. Suzuki *et al.*, *J. Chem. Phys.*, 2010, **132**, 174302]. We constructed adiabatic and diabatic potential energy surfaces of these $\pi\pi^*$ and $n\pi^*$ states using the multireference configuration interaction method and calculated their diabatic couplings within two-dimensional subspaces spanned by selected ground-state normal coordinates. Contrary to the surface hopping study, our nuclear wave packet simulations demonstrated that nonadiabatic transitions to the S_3 and S_4 states are so small that the conventional two-state (S_1 and S_2) picture is valid. Ultrafast internal conversion of pyrazine, which is deemed to proceed with a 22 fs lifetime, in fact consists of three consecutive steps: (i) The wave packet excited to the S_2 state travels toward the $S_2 - S_1$ conical intersection in 10 fs, (ii) the nonadiabatic transition to the S_1 state progresses at a rapid rate corresponding to a transient lifetime of 7 fs, and (iii) intramolecular vibrational energy redistribution occurs in the S_1 state in about 80 fs

after optical excitation. To verify this prediction, time-resolved experiments with a resolution of several fs or shorter are desirable.

1 Introduction

Pyrazine $C_4H_4N_2$ is a typical azabenzene that undergoes ultrafast nonradiative transitions.¹⁻³ Determination of their origins and rates has been one of the hot subjects in both molecular spectroscopy and photo-dynamical theory.⁴⁻⁷ Pyrazine is also a typical target molecule for coherent control to demonstrate almost complete suppression or acceleration of ultrafast nonradiative processes.⁸⁻¹¹ Evidence of the ultrafast nonradiative transitions was found in diffuse bands in the $S_2 \leftarrow S_0$ absorption spectrum, and an extremely fast nonradiative decay channel was observed in the emission excitation spectrum above $35,000 \text{ cm}^{-1}$.⁶ Results of time-resolved spectroscopic experiments to directly measure nonradiative decay constants were also reported.^{12,13} Domcke and coworkers theoretically proposed that the ultrafast nonradiative transition is due to internal conversion from the optically bright S_2 ($^1B_{2u}, \pi\pi^*$) to the optically dark S_1 ($^1B_{3u}, n\pi^*$) state through their conical intersection (CI). The calculations by Domcke and coworkers were carried out within a restricted vibrational mode model by using semi-empirical¹⁴⁻¹⁹ and *ab initio*²⁰⁻²² molecular orbital (MO) methods. The diffuse band structure in the $S_2 \leftarrow S_0$ absorption spectrum was simulated by taking into account multi-mode effects and introducing a phenomenological broadening parameter under the assumption of an exponential decay.²³⁻³²

Concerning the origin of the ultrafast nonradiative transitions in pyrazine, we especially pay our attention to the experimental and theoretical results presented by Suzuki *et al.*¹³ and Werner *et al.*,^{30,33} respectively. Suzuki *et al.* measured the lifetime of $22 \pm 3 \text{ fs}$ for the S_2 state by real-time resolved pump-probe photoelectron spectroscopy.¹³ The value was obtained by fitting the

photoelectron signals to a single exponential decay form; however, the cross correlation time between the pump and probe pulses was 22 fs as well. This means that the measured value of the S_2 lifetime is the same as the time resolution of the experiment and hence there remains the possibility of faster transition rates. They also observed vibrational quantum beats in the photoelectron signals. The Fourier transform of the quantum beats exhibited a frequency component of $560 \pm 40 \text{ cm}^{-1}$, which agrees with the vibrational frequency of the totally symmetric a_g mode often denoted as Q_{6a} in the S_1 state (583 cm^{-1}). This indicates that vibrational coherence is maintained in this mode even after the nonradiative transition.

Werner *et al.* raised a fundamental question about ultrafast nonradiative transition pathways of pyrazine.³⁰ They proposed new nonradiative transition pathways via optically dark states, S_3 ($^1A_u, n\pi^*$) and S_4 ($^1B_{2g}, n\pi^*$), in addition to the direct pathway from S_2 to S_1 . The terminologies of S_3 and S_4 are based on the order of their electronic energies observed at the Franck-Condon position. These states were not considered in most of the previous theoretical works.¹⁴⁻²⁸ The two dark states, S_3 and S_4 , theoretically predicted to locate near the S_1 state³⁴ were experimentally observed by near-threshold electron energy-loss³⁵ and UV-IR fluorescence dip³⁶ spectroscopies, respectively, instead of UV absorption. Werner *et al.* calculated time-dependent populations of the two dark states in addition to the S_1 and S_2 states by using the “on-the-fly” time-dependent density functional theory (TDDFT). Here, nonadiabatic transitions were treated with Tully’s stochastic fewest switches surface hopping procedure.³⁷ Their analysis of the calculated time-resolved photoelectron spectrum of pyrazine, averaged over 60 trajectories obtained from the nonadiabatic dynamics, showed that

the decay of the S_2 state occurs on a timescale of 20 fs. The lifetime of the S_2 state was estimated to be 21.1 fs by fitting the time-dependent S_2 population to a single exponential decay form. A further examination of the calculated time-dependent populations after excitation to the S_2 state showed that almost 60 % of the initial S_2 population was preferentially transferred to both the S_3 and S_4 states rather than to the S_1 state at the initial stage of nonradiative transition (0 ~ 10 fs). The calculated lifetime of the S_2 state is quite close to the experimental values of 20 ± 10 fs by Stert *et al.*¹² and 22 ± 3 fs by Suzuki *et al.*¹³ as well as the theoretical value of about 20 fs.^{24,26,27} It should be noted that the experimental and theoretical values of the lifetime, which were referred to for comparison with that calculated by Werner *et al.*, were obtained for the $S_2 \rightarrow S_1$ nonradiative process without considering the S_3 and S_4 states. This means that the mechanism of ultrafast nonradiative transition in pyrazine still remains unclear. At present, there is no answer to the question why such almost the same value was obtained for the lifetime by Werner *et al.* and those by others even though the different models were adopted. Very recently, Sala *et al.* reported the results of the multiconfiguration time-dependent Hartree (MCTDH) calculation including the four excited states in a 16-mode model Hamiltonian constructed using the extended multiconfiguration quasi-degenerate second-order perturbation theory (XMCQDPT2), which suggested a noticeable participation of the S_3 state but not of the S_4 state in nonradiative transition pathways.³¹ This makes it more difficult to paint a true picture of ultrafast nonradiative transition in photoexcited pyrazine.

It should also be noted that for the case in which a CI between two excited states locates at a position far from the Franck-Condon region their populations in general exhibit a non-exponential

time-dependent behavior. This is because the nuclear wave packet (WP) initially created in one of the two excited states by an ultrashort laser pulse moves on its potential energy surface (PES) toward the CI to transfer to the other excited state. The WP dynamics can be regarded as consisting of three consecutive processes: (i) The WP propagation (dephasing) on the initial PES, (ii) the transfer of the WP to the other excited state through the CI, and (iii) the subsequent propagation on the other PES. If this is the case, we desire to figure out the time constants of the individual processes (especially the rate for the second one).

In this paper, to solve the problems described above, we present the results of *ab initio* quantum dynamical simulations of ultrafast nonradiative transitions in pyrazine taking into account the S_3 and S_4 states in addition to the S_1 and S_2 states. First, the CIs associated with the S_3 (S_4) and S_2 states are determined as well as that between the S_1 and S_2 states since they may play an essential role in ultrafast processes occurring within 10 fs. Then, the time development of the Franck-Condon WP initially prepared on the S_2 PES is scrutinized. The analysis of the calculated time-dependent populations of the excited states quantifies the participations of the S_3 and S_4 states in nonradiative transition pathways and reveals that the S_2 population exhibits a non-exponential time-dependent behavior. From these results, we acquire the information on the time required for the WP to arrive at the most relevant CI after pulse excitation, the transient rate of the ultrafast nonradiative transition via the CI, and the timescale of vibrational energy localization.

In Section 2, the *ab initio* quantum dynamical approach adopted in this work is briefly described. The highly accurate multireference configuration interaction (MRCI) method, which has been

successfully applied to the search for CIs in heteroaromatic nucleobases,^{38,39} was utilized for PES calculations. To properly simulate coherent nuclear dynamics on the excited-state PESs coupled by CIs, we employed the nuclear WP propagation method within a minimum vibrational mode model in which an effective tuning mode and coupling modes are involved. It should be applicable to the initial stage of ultrafast nonradiative transitions in pyrazine where a large part of the initial vibrational energy remains localized in a few specific vibrational modes. In fact, excited-state nuclear dynamics in pyrazine keeps a localized WP character even after the WP passes through a CI since quantum beats of the tuning mode can be seen in time-resolved photoelectron signals.¹³ In Section 3, first, the calculated PESs and CIs involving the optically dark S_3 and S_4 states as well as the optically bright S_2 and almost dark S_1 states are presented. Second, we show the nuclear WP propagations in three nonradiative transition pathways from the S_2 state. The results in this paper are compared with those by Werner *et al.*³⁰ and Sala *et al.*³¹ The role of CIs in ultrafast nonradiative transitions in pyrazine is clarified. The validity and limitation of the minimum vibrational mode model that we used are also discussed. Finally, in Section 4, we conclude this paper with a short remark on time-resolved spectroscopy for directly probing ultrafast nonradiative molecular processes.

2 Computational outline

2.1 Geometry optimization and excited-state calculation

Electronic structure calculations were carried out with the 6-311++G** Gaussian basis set⁴⁰ by

using the *ab initio* quantum chemistry program MOLPRO.^{41,42} The geometry of pyrazine was optimized in the electronic ground state S_0 (1A_g) under D_{2h} symmetry constraints at the complete-active-space self-consistent field (CASSCF)^{43,44} level of theory. The active space was composed of ten electrons distributed among eight orbitals (three π , three π^* , and two lone-pair orbitals). The lowest five singlet electronic states (S_0 to S_4) were state-averaged with equal weights to guarantee a balanced description. Harmonic vibrational frequencies of normal modes were subsequently computed at the optimized geometry. To take dynamical electron correlation into account, the CASSCF energies were refined at the level of the internally contracted MRCI including single and double excitations to the external space (MRCISD).⁴⁵⁻⁴⁷ The six inner-shell orbitals were chosen as frozen-core orbitals, which were doubly occupied in all configurations, to reduce computational effort. The validity of this CASSCF/MRCISD treatment to evaluate the electronic structure of pyrazine will be assessed by comparing the calculated results with the experimental data of geometrical parameters, vibrational frequencies, and excitation energies in Section 3.1.

2.2 Effective vibrational degrees of freedom for nuclear WP simulations

In preparation for nuclear WP simulations within a minimum vibrational mode model, we selected effective vibrational degrees of freedom from symmetry consideration of the so-called \mathbf{g} and \mathbf{h} vectors developed by Yarkony.⁴⁸⁻⁵⁰ The \mathbf{g} and \mathbf{h} vectors span the branching plane of a CI. The former is given by the gradient of the energy difference between two crossing states at the CI; the latter is the nonadiabatic coupling vector, which is equivalent to the derivative coupling times the

energy difference between the two states. From these definitions, the vibrational modes that contribute to the \mathbf{h} vector couple the electronic states and are thus termed coupling modes; those involved in the \mathbf{g} vector tune the separation of their PESs and are hereafter referred to as tuning modes.

Two-dimensional PESs were constructed within the subspaces defined by relevant tuning and coupling modes for the $S_3 - S_2$ and $S_2 - S_1$ nonadiabatic transitions on which our particular attention is focused. From symmetry requirement, the \mathbf{g} vector or tuning modes must be totally symmetric. Previous experimental^{4,6} and theoretical^{20,21} studies in the past few decades suggested that the three totally symmetric a_g normal modes, Q_1 , Q_{6a} , and Q_{9a} , are dominant tuning modes for the $S_2 \leftarrow S_0$ photoabsorption. Besides, the quantum beats observed in the time-resolved photoelectron imaging measurement implied that only the Q_{6a} mode was coherently excited by ultrashort femtosecond UV laser pulses.¹³ We adopted, therefore, the Q_{6a} normal mode in the S_0 state as the most relevant tuning mode for both the $S_3 - S_2$ and $S_2 - S_1$ transitions. On the other hand, the symmetry of the \mathbf{h} vector or coupling modes depends on the symmetries of the intersecting states. It is well known that out of the 24 vibrational modes of pyrazine only the Q_{10a} mode (b_{1g}) couples the S_2 (${}^1B_{2u}$) and S_1 (${}^1B_{3u}$) states. The coupling modes between the S_3 (1A_u) and S_2 (${}^1B_{2u}$) states should belong to the b_{2g} symmetry species and there are two b_{2g} modes denoted as Q_4 and Q_5 . The two-dimensional excited-state PESs were obtained within the $Q_{6a} - Q_{10a}$, $Q_{6a} - Q_4$, and $Q_{6a} - Q_5$ subspaces at the MRCISD level of theory.

2.3 Nuclear WP propagation for nonadiabatic dynamics

We explored quantum dynamics of the initially prepared Franck-Condon WP on the two-dimensional coupled PESs. The vibrational ground-state wave function in the S_0 state was placed on the PES of the optically bright S_2 state at the initial time $t = 0$. The subsequent time evolution of the WP was performed in the diabatic basis to deal with nonadiabatic couplings as in our previous studies on laser-driven ultrafast electron-nuclear dynamics in pyrazine derivatives.⁵¹⁻⁵⁵ Exact adiabatic-to-diabatic transformation requires the line integral of the derivative coupling matrix, which is in general path dependent for polyatomic molecules.^{56,57} We instead used the quasi-diabatization scheme available in MOLPRO that is based on an analysis of configuration interaction vectors.⁵⁸ The total wave function of pyrazine was expanded in terms of diabatic electronic states, each of which is a linear combination of adiabatic ones. The expansion coefficients or diabatic nuclear wave functions $\psi_m(\mathbf{Q}, t)$, where \mathbf{Q} is the two-dimensional mass-weighted normal coordinate vector, can be propagated by solving the coupled equations⁵⁹

$$i\hbar \frac{\partial}{\partial t} \psi_m(\mathbf{Q}, t) = -\frac{\hbar^2}{2} \nabla^2 \psi_m(\mathbf{Q}, t) + \sum_n V_{mn}(\mathbf{Q}) \psi_n(\mathbf{Q}, t), \quad (1)$$

where \hbar is the Dirac constant and ∇^2 is the Laplace operator with respect to \mathbf{Q} . $V_{mn}(\mathbf{Q})$ represent diabatic potentials for $m = n$ and couplings for $m \neq n$. The differential equations (1) were integrated numerically by means of the split-operator method⁶⁰ with the fast Fourier transform algorithm. The resultant diabatic WPs $\psi_m(\mathbf{Q}, t)$ were converted to adiabatic WPs $\chi_m(\mathbf{Q}, t)$ as

$$\chi_m(\mathbf{Q}, t) = \sum_n U_{mn}(\mathbf{Q}) \psi_n(\mathbf{Q}, t), \quad (2)$$

where the orthogonal transformation matrix $U_{mn}(\mathbf{Q})$ was obtained from the above-mentioned

quasi-diabatization scheme.

3 Results and discussion

3.1 Electronic structure at the optimized geometry

We first present the geometrical parameters in the S_0 state of pyrazine computed at the CASSCF/6-311++G** level of theory. The D_{2h} optimized geometry is displayed in Fig. 1 and the bond lengths and angles at this geometry are compared to the experimental data reported by Cradock *et al.*⁶¹ in Table 1. The calculated results are in good accord with the experimental ones.

The vibrational vectors of the Q_{6a} , Q_{10a} , Q_4 , and Q_5 modes obtained from the normal mode calculation are illustrated schematically in Fig. 1. The tuning mode Q_{6a} (a_g) corresponds to a totally symmetric in-plane ring deformation. The Q_{10a} (b_{1g}) and Q_5 (b_{2g}) modes involve an out-of-plane CH bending vibration. In the former, neighboring CH bonds move in the same direction; in the latter, they move in opposite directions. The remaining coupling mode Q_4 (b_{2g}) represents an out-of-plane ring bending. The CASSCF harmonic vibrational frequencies of the four modes are listed in Table 2. For all of them, the calculated frequency is slightly higher than the experimental one but the difference is only less than 50 cm^{-1} . The agreement is especially good for the Q_4 and Q_5 modes. The consistency in geometrical parameters and vibrational frequencies between experiment and theory exemplifies the adequacy of the CASSCF/6-311++G** calculations for the evaluation of the ground-state properties of pyrazine.

Table 3 provides the present CASSCF and MRCISD vertical excitation energies to the lowest

four singlet excited states along with available experimental and other theoretical values. Among the four theoretical methods in Table 3, only the MRCISD results successfully reproduced the experimentally determined order of the excited states: S_1 ($^1B_{3u}$), S_2 ($^1B_{2u}$), S_3 (1A_u), and S_4 ($^1B_{2g}$). Throughout the present paper, the nomenclature S_1 to S_4 designates this order of the excited states at the optimized geometry. The CASSCF method overestimates the S_3 state to be highest, while it is located below the S_2 state in the TDDFT³⁰ and XMCQDPT2³¹ calculations. From literature data,^{29,31,62} computational methods based on a perturbation theory including the linear-response TDDFT and XMCQDPT2 tend to underestimate the S_3 state and give a wrong order of the excited states unlike the MRCISD, which is a variational method. Although the MRCISD vertical excitation energies in Table 3 are all higher than the respective experimental ones, the difference is not very large (no more than about 0.7 eV) and comparable among the four excited states. For the purpose of elucidating nonadiabatic transition dynamics from the optically bright $\pi\pi^*$ to dark $n\pi^*$ states of pyrazine, the energies of the latter relative to the former should be important rather than their excitation energies from the S_0 state. The experimental relative energies are reproduced reasonably well in the MRCISD case. The accuracy of the energy calculation is expected to be improved by extending the active space and/or involving triple or more excitations, which is, however, computationally demanding. Therefore the MRCISD method offers an optimal balance between computational cost and accuracy for excited-state calculations of pyrazine. In Table 3, the presence of the S_3 state in the energetic neighborhood of the S_2 state suggests a potential crossing between them near the optimized geometry.

3.2 Potential energy curves along the tuning mode Q_{6a}

In general, nuclear displacements along a totally symmetric tuning mode preserve the symmetry of a molecule and hence electronic states with different irreducible representations can cross each other in this direction, forming a symmetry-allowed CI in a two-dimensional space spanned by tuning and coupling modes. In this context, to locate potential crossings between the $\pi\pi^*$ and $n\pi^*$ states of pyrazine, we computed one-dimensional cuts of its excited-state PESs along the tuning mode Q_{6a} . The one-dimensional TDDFT PESs of the four excited states that we calculated with the same functional and basis set (B3LYP/TZVP) as in ref. 30 by using the Gaussian 09 program package⁶⁴ are depicted in Fig. 2a for comparison with the CASSCF and MRCISD PESs in Figs. 2b and 2c, respectively. Also shown in Fig. 2c is the probability density of the Franck-Condon WP. The shape of each PES is similar but its absolute value is different among the three theoretical results as expected from the discussion in Section 3.1. The crossings between the TDDFT PESs are located at entirely different positions from those in the CASSCF and MRCISD cases mainly because of the overestimation of the S_2 PES and the underestimation of the S_3 PES: the $S_4 - S_2$ crossing in the close vicinity of the optimized geometry $Q_{6a} = 0$, the $S_3 - S_2$ crossing in the negative region of Q_{6a} , and the $S_2 - S_1$ crossing far away from the Franck-Condon region. The MRCISD PESs of the S_1 and S_3 states are greatly lowered by the inclusion of dynamical electron correlation compared to the respective CASSCF PESs. As a consequence, the energy difference between the S_2 and S_1 states in the Franck-Condon region is larger and thereby their crossing point appears farther from the optimized geometry in the MRCISD case. Moreover, the order of the S_3 and S_4 states is reversed not

only in the vicinity of the optimized geometry but in most of the region shown in Fig. 2. This gives birth to the crossings of the S_3 state with the S_2 and S_4 states, which are absent in the CASSCF case. The CASSCF PESs of the S_2 and S_1 states have already been surveyed by Woywod *et al.*²¹ but our calculations illuminated the necessity of dynamical electron correlation at the MRCI level to accurately construct the PESs of pyrazine and identify their CIs. In the following, we advance detailed discussions on the MRCISD results.

In Fig. 2c, the optically bright S_2 state intersects all the three optically dark states, S_1 , S_3 , and S_4 . The S_3 and S_2 states are degenerate at $Q_{6a} = 0.64 u^{1/2} a_0$ with u and a_0 being the unified atomic mass unit and the Bohr radius, respectively, inside the Franck-Condon region as expected, while the $S_4 - S_2$ and $S_2 - S_1$ crossings are located at $Q_{6a} = 1.10$ and $-1.21 u^{1/2} a_0$, respectively, outside the Franck-Condon region. Without nonadiabatic couplings, the WP generated on the S_2 PES by a laser pulse should travel toward the $S_2 - S_1$ crossing. The S_4 state is higher in energy than the S_3 state during the course of propagation to the $S_2 - S_1$ crossing. Unless a substantial population transfer to the S_3 state takes place by nonadiabatic transition, it is reasonable to conclude that the S_4 state plays a minor role in ultrafast internal conversion of pyrazine. To clarify this issue, we investigated the subsequent time evolution of the Franck-Condon WP including the coupling modes between the S_3 and S_2 states, which will be presented in Section 3.3.

3.3 WP dynamics for the $S_3 - S_2$ nonradiative transition

3.3.1 $Q_{6a} - Q_4$ subspace

Out of the two b_{2g} modes of pyrazine, which couple the S_3 and S_2 states, the Q_4 mode was first

employed in a nuclear WP simulation. Vibrational motions along the Q_4 mode lower the symmetry of the molecule to the C_{2h} point group, where the C_2 axis bisects the two CC bonds. The electronic states connected to S_0 (1A_g), S_1 ($^1B_{3u}$), S_2 ($^1B_{2u}$), S_3 (1A_u), and S_4 ($^1B_{2g}$) at the D_{2h} optimized geometry are associated with the irreducible representations 1A_g , 1B_u , 1A_u , 1A_u , and 1A_g , respectively, for C_{2h} pyrazine with $Q_4 \neq 0$. The two-dimensional MRCISD adiabatic PESs of the two 1A_u states with respect to the CASSCF normal coordinates $\mathbf{Q} = (Q_{6a}, Q_4)$ are depicted in Fig. 3a. The S_1 state is excluded since no transition occurs from either S_2 or S_3 to S_1 in this subspace. The adiabatic PESs in Fig. 3a exhibit a gentle curve in the Q_4 direction compared to a relatively steep rise with respect to Q_{6a} . A close-up view in Fig. 3b clearly shows a CI at $\mathbf{Q} = (0.64 \text{ u}^{1/2}a_0, 0)$ as mentioned in Section 3.2. Figures 3c and 3d display the diabatic PESs of the two 1A_u states and their diabatic coupling, respectively. In the former, the cusp at the $S_3 - S_2$ CI has been removed and the diabatic PESs are smooth differentiable functions of \mathbf{Q} that intersect each other; in the latter, the diabatic coupling is zero for $Q_4 = 0$, where the adiabatic and diabatic electronic states are identical to each other. The diabatic coupling is less dependent on Q_{6a} and varies almost linearly with Q_4 in the region shown in Fig. 3d. The slope in the Q_4 direction is larger as Q_{6a} increases. The split-operator propagation of the Franck-Condon WP within the $Q_{6a} - Q_4$ subspace was executed using the diabatic PESs and coupling in Figs. 3c and 3d, respectively. For both the two modes, the domain $[-5.0 \text{ u}^{1/2}a_0, 5.0 \text{ u}^{1/2}a_0]$ was uniformly discretized into 64 grid intervals so as to represent numerical wave functions. The time increment for the WP propagation was 0.0024 fs (2.4 as). The numerical results are analyzed in the adiabatic basis in the following paragraphs.

The population of the (adiabatic) S_3 state defined as

$$P_3(t) \equiv \int |\chi_3(\mathbf{Q}, t)|^2 d\mathbf{Q} \quad (3)$$

is plotted as a function of time in Fig. 4; that of the S_2 state is given by $P_2(t) = 1 - P_3(t)$. A small fraction of the initial S_2 population is transferred to the S_3 state and $P_3(t)$ reaches its maximum at $t = 5.2$ fs, which is, however, less than 0.03. This value is much smaller than the maximum populations of the S_3 state in the on-the-fly surface hopping calculation combined with the TDDFT³⁰ and the 16-mode MCTDH calculation based on the XMCQDPT2,³¹ which are about 0.4 and 0.5, respectively. The population $P_3(t)$ falls sharply to even below 0.01 at $t \sim 11$ fs because of a reverse transition to the S_2 state and then continues to decrease gradually. This indicates that the nonadiabatic coupling between the S_3 and S_2 states induced by the Q_4 vibration is not strong enough to transfer a significant amount of the population to the S_3 state. Consequently, most of the population remains in the S_2 state in the present simulation within the $Q_{6a} - Q_4$ subspace.

The time evolution of the S_2 WP is shown in Fig. 5. The trajectory of the expectation value of the normal coordinate \mathbf{Q} ,

$$\mathbf{Q}_2(t) \equiv P_2(t)^{-1} \int \mathbf{Q} |\chi_2(\mathbf{Q}, t)|^2 d\mathbf{Q}, \quad (4)$$

is drawn in Fig. 5 as well for the manifestation of the WP motion. After excitation at $t = 0$, the Franck-Condon WP starts to move in the negative direction of Q_{6a} following the gradient of the S_2 PES, while expanding along the other mode Q_4 where the PES is quite shallow. At $t \sim 10$ fs, the WP approaches the $S_2 - S_1$ crossing point at $\mathbf{Q} = (-1.21 \text{ u}^{1/2} a_0, 0)$. The center of $\chi_2(\mathbf{Q}, t)$, $\mathbf{Q}_2(t)$, reaches

the crossing point at $t \sim 20$ fs and in the next 20 fs the WP is reflected by a potential energy barrier, contracting again and passing back through the crossing point. Eventually, the WP simply oscillates, exhibiting no signature of the coupling with the S_3 state as anticipated from the very small population in Fig. 4. As far as the Q_{6a} and Q_4 modes are concerned, the Franck-Condon WP runs on the S_2 PES toward the $S_2 - S_1$ CI almost without transition to the other $n\pi^*$ states.

3.3.2 $Q_{6a} - Q_5$ subspace

Next, we considered the nonadiabatic coupling between the S_3 and S_2 states caused by the other b_{2g} mode Q_5 . Upon the movement in this direction, pyrazine has the same C_{2h} symmetry as in the case of the Q_4 mode and accordingly the irreducible representation of the S_2 state changes to 1A_u . Figure 6a displays the adiabatic PESs of the two 1A_u states with respect to the two-dimensional normal coordinates $\mathbf{Q} = (Q_{6a}, Q_5)$. The two adiabatic PESs increase more quickly in the Q_5 direction than in the Q_4 direction in Fig. 3a. In marked distinction from the Q_4 case, the separation of the adiabatic PESs is extremely small irrespective of the displacement from the $S_3 - S_2$ CI at $\mathbf{Q} = (0.64 \text{ u}^{1/2} a_0, 0)$ along the Q_5 mode as evidently seen in a magnified view in Fig. 6b. The diabatic PESs and coupling, which were used for the propagation of the Franck-Condon WP, are shown in Figs. 6c and 6d, respectively. The magnitude of the diabatic coupling is rather small in a wide range of \mathbf{Q} ; it is almost zero in the negative region of Q_{6a} .

Figure 7 depicts the temporal change in the population $P_3(t)$ calculated by the integration of the probability density $|\chi_3(\mathbf{Q}, t)|^2$ over the $Q_{6a} - Q_5$ subspace as in eqn (3). It behaves similarly to that in Fig. 4: The peak value of $P_3(t)$ is below 0.03 at $t \sim 5$ fs and then it declines to less than 0.01. A little

difference from the Q_4 case is a small recovery at $t > 23$ fs arising from repeated transitions between the S_3 and S_2 states. The time development of the S_2 WP in this subspace, which is illustrated in Fig. 8, also resembles that in Fig. 5. The WP touches the $S_2 - S_1$ crossing point in about 10 fs and afterwards exhibits a back-and-forth motion along the Q_{6a} mode, although it does not spread out in the Q_5 direction where the potential well is deep. The results in Figs. 7 and 8 evidence negligible participations of the S_3 and S_4 states in nonradiative transition pathways.

Our PES calculations and quantum WP simulations contradict the prediction in the on-the-fly surface hopping study in the framework of the TDDFT that nonadiabatic transitions to the optically dark S_3 and S_4 states are dominant at the early stage of nonradiative transition in pyrazine.³⁰ One possible reason for this contradiction is the incorrect evaluation of relative excited-state energies in the TDDFT discussed in Sections 3.1 and 3.2: The existences of the $S_3 - S_2$ CI on the way down the S_2 PES and the $S_4 - S_2$ CI in the proximity of the optimized geometry shown in Fig. 2a should lead to preferred transitions to the S_3 and S_4 states, respectively. Another possibility is an inappropriate treatment of quantum coherence in the surface hopping method. The present results are partly but not fully consistent with those of the 16-mode MCTDH calculation based on the XMCQDPT2, which suggested a central role of the S_3 state and the unimportance of the S_4 state in ultrafast nonradiative transition.³¹ In the XMCQDPT2, the S_4 state lies about 0.6 eV above the S_2 state at the optimized geometry as tabulated in Table 3, forming their CI far enough from there. On the other hand, the vertical excitation energy to the S_3 state was adjusted at 4.69 eV so as to obtain a reasonable absorption spectrum from the MCTDH calculation in ref. 31. This brought the $S_3 - S_2$ CI

very close to the optimized geometry, inducing a prompt transition to the S_3 state. Besides, as implied in ref. 31, the non-negligible deviations of the PESs derived from a linear coupling model Hamiltonian from the *ab initio* ones may have affected the MCTDH results as well. The accuracy of electronic structure calculations is crucial even for the qualitative description of excited-state nuclear dynamics in pyrazine.

3.4 WP dynamics for the $S_2 - S_1$ nonradiative transition

The results presented in the previous sections have corroborated that the S_3 and S_4 states make minor contributions to ultrafast internal conversion of pyrazine. For detailed analysis of the internal conversion process, we also examined the $S_2 - S_1$ nonadiabatic relaxation dynamics within the $Q_{6a} - Q_{10a}$ subspace. As mentioned above, the Q_{10a} mode is the only b_{1g} normal mode of D_{2h} pyrazine, which couples the lowest two excited states. With nonzero displacements along this mode, the molecular symmetry is lowered to the C_{2h} point group as in the previous cases; however, the orientation of the principal axis is different. In this case, the C_2 axis connects the two nitrogen atoms. For $Q_{10a} \neq 0$, the S_1 and S_2 states belong to the 1B_u symmetry species, while those of the S_0 , S_3 , and S_4 states are 1A_g , 1A_u , and 1B_g , respectively. Figure 9a shows the two-dimensional adiabatic PESs of the two 1B_u states within the $Q_{6a} - Q_{10a}$ subspace in which $\mathbf{Q} = (Q_{6a}, Q_{10a})$. The $S_2 - S_1$ CI at $\mathbf{Q} = (-1.21 \text{ u}^{1/2} a_0, 0)$ is difficult to identify in an overhead view in Fig. 9a; a close-up view in Fig. 9b confirms a double-cone shape of the adiabatic PESs near the CI. The corresponding diabatic PESs and coupling are depicted in Figs. 9c and 9d, respectively. The diabatic coupling is almost independent of Q_{6a} but grows drastically with Q_{10a} in the region shown in Fig. 9d.

The time-dependent S_2 population, $P_2(t)$, obtained from the nuclear WP simulation within the $Q_{6a} - Q_{10a}$ subspace is plotted in Fig. 10a. In the time range shown in Fig. 10, the temporal behavior of $P_2(t)$ is analogous to that in the time-dependent discrete variable representation (TDDVR) calculation with a 24-mode model Hamiltonian by Puzari *et al.*,²⁷ which is given in Fig. 10b. This agreement suggests that out of the 24 vibrational modes of pyrazine the two modes Q_{6a} and Q_{10a} are of primary importance at the initial stage of nonradiative transition, which justifies our theoretical treatment based on the minimum vibrational mode model. The lifetime of the S_2 state evaluated from an exponential decay fit of $P_2(t)$ in Fig. 10a is 19.4 fs, which is consistent with the experimental value of 22 ± 3 fs.¹³ Nevertheless, the curve of $P_2(t)$ deviates significantly from a simple exponential decay. It is also dissimilar to that in the on-the-fly surface hopping calculation combined with the TDDFT³⁰ shown in Fig. 10b, which fits well to an exponential function with a 21.1 fs lifetime. As pointed out in Section 1, the non-exponential time-dependent behavior of $P_2(t)$ indicates that the $S_2 - S_1$ relaxation dynamics can be distinctly divided into three consecutive processes, namely, (i) the WP motion on the S_2 PES, (ii) nonadiabatic transition via the $S_2 - S_1$ CI, and (iii) the subsequent propagation on the S_1 PES. The three-step mechanism is supported by the existence of the CI outside the Franck-Condon region shown in Fig. 2c. Roughly speaking, the boundaries between the three time domains of nonradiative transition are found at $t = 10$ and 30 fs; we refer to the three time domains as Domains 1, 2, and 3.

For further investigation of the $S_2 - S_1$ internal conversion dynamics, let us carefully analyze the temporal variation of $P_2(t)$ in the respective time domains as well as those of the probability

densities $|\chi_2(\mathbf{Q}, t)|^2$ and $|\chi_1(\mathbf{Q}, t)|^2$ in the $Q_{6a} - Q_{10a}$ subspace displayed in Fig. 11. In Domain 1, the Franck-Condon WP runs down the S_2 PES and there is almost no transfer of the WP to the S_1 state before the front portion of $\chi_2(\mathbf{Q}, t)$ enters the $S_2 - S_1$ CI region at $t \sim 10$ fs. More than 0.94 of the population still remains in the S_2 state until $t = 10$ fs. In Domain 2, $P_2(t)$ drops dramatically by nonadiabatic transition. The snapshot at $t = 19.4$ fs in Fig. 11, which is in the midst of the population transfer, illustrates the decay of the S_2 WP and the concomitant growth of the S_1 WP. At $t > 21$ fs, $P_1(t)$ exceeds 0.5, that is, it becomes larger than $P_2(t)$. The transient rate of the $S_2 - S_1$ nonadiabatic transition in the range [21 fs, 27 fs] where $P_2(t)$ can be perfectly approximated by a single exponential function is 0.13 fs^{-1} corresponding to a lifetime of 7.4 fs. The transient rate, which is much faster than the overall rate of transition evaluated by exponential fitting over the whole range [0, 40 fs], was not quantified in the paper by Puzari *et al.*²⁷ The WP transferred to the S_1 state bifurcates to avoid the CI at $\mathbf{Q} = (-1.21 \text{ u}^{1/2} a_0, 0)$ as seen in the snapshot at $t = 29.0$ fs in Fig. 11. In Domain 3, the two bifurcated portions of $\chi_1(\mathbf{Q}, t)$ move adiabatically on the S_1 PES, acquiring opposite geometric (or Berry) phases.⁶⁵ The snapshot at $t = 38.7$ fs in Fig. 11 clearly exhibits a node due to the destructive interference between them, while the average position $\mathbf{Q}_1(t)$ always lies on the Q_{6a} axis. Finally, the S_1 population reaches 0.90 at $t = 40$ fs.

Do the adiabatic passages of the WPs continue in the rest of Domain 3, that is, at $t > 40$ fs in the $Q_{6a} - Q_{10a}$ subspace? Figure 12 shows the subsequent behavior of $P_2(t)$ in the range [40 fs, 120 fs]. A strong recurrence begins at $t \sim 80$ fs when the WPs return to the $S_2 - S_1$ CI region. The value of $P_2(t)$ at $t \sim 100$ fs is more than 0.4. In contrast, recurrence of the S_2 population is negligibly small

and it asymptotically approaches to zero in the TDDVR calculation which included all the vibrational degrees of freedom of pyrazine in a quadratic coupling model Hamiltonian.²⁷ This discrepancy implies that under the multi-mode condition the vibrational energy initially localized in the Q_{6a} and Q_{10a} modes is redistributed among the other modes to excite them before $t \sim 80$ fs, preventing the return of the WPs to the CI and thus the reverse population transfer to the S_2 state. The occurrence of intramolecular vibrational energy redistribution (IVR) presumably at $t \sim 80$ fs tells us that the validity of the minimum vibrational mode model is limited to this time period.

Reverting to Table 3, the energy difference between the lowest two excited states at the optimized geometry is slightly underestimated from the experimental one. The location of the $S_2 - S_1$ CI may be actually farther from the Franck-Condon region than in Fig. 2c. In addition, the WP created in the optically bright S_2 state by a femtosecond laser pulse should be spatially narrower than the Franck-Condon WP. For these reasons, it may take a little longer than 10 fs for the S_2 WP to arrive at the CI for femtosecond pulse excitations. This reinforces the three-step mechanism of ultrafast nonradiative transition in photoexcited pyrazine. Yet, the durations of the pump and probe pulses in the time-resolved photoelectron imaging measurement by Suzuki *et al.*¹³ were 14 and 17 fs, respectively, which are longer than the arrival time of about 10 fs to the CI and the transient lifetime of 7 fs for the nonadiabatic transition via the CI. The WP evolves and the $S_2 - S_1$ nonadiabatic transition progresses during irradiation. We speculate that the spectroscopy with a 22 fs time resolution was unable to resolve the three ultrafast processes (*i.e.*, the ones in Domains 1, 2, and 3) and that the measured S_2 lifetime of 22 ± 3 fs corresponds to the overall rate of these processes as

shown above.

4 Conclusions

We have theoretically examined the contributions of the low-lying $n\pi^*$ excited states S_1 (${}^1B_{3u}$), S_3 (1A_u), and S_4 (${}^1B_{2g}$) to ultrafast nonradiative transition from the lowest $\pi\pi^*$ excited state S_2 (${}^1B_{2u}$) in pyrazine by *ab initio* quantum dynamical calculations. Our CASSCF/MRCISD electronic structure computations accurately reproduced the experimental data of the equilibrium geometry, vibrational frequencies, and excitation energies of pyrazine. Adiabatic PESs along the most relevant tuning mode Q_{6a} identified crossings between the optically bright $\pi\pi^*$ and dark $n\pi^*$ states. The absence of the $S_4 - S_2$ crossing in the Franck-Condon region suggests a negligible participation of the S_4 state in nonradiative transition pathways. The nuclear WP simulations on the two-dimensional PESs within the $Q_{6a} - Q_4$ and $Q_{6a} - Q_5$ subspaces confirmed that the $S_3 - S_2$ nonadiabatic transition is vanishingly small and thus support the conventional two-state (S_1 and S_2) picture. These findings disagree entirely with the on-the-fly semiclassical surface hopping study in the framework of the TDDFT, which claimed that nonadiabatic transitions to the S_3 and S_4 states take place predominantly at the early stage of electronic relaxation in pyrazine,³⁰ and partly with the MCTDH study based on the XMCQDPT2, which affirmed it for the S_3 state only.³¹ The poor accuracies of the TDDFT and XMCQDPT2 in excited-state calculations of pyrazine are likely to be responsible for the failures of the surface hopping and MCTDH approaches, respectively. Furthermore, the nuclear WP simulation within the $Q_{6a} - Q_{10a}$ subspace revealed that ultrafast internal conversion of

pyrazine proceeds in three consecutive steps: (i) The WP generated on the S_2 PES reaches the $S_2 - S_1$ CI in 10 fs, (ii) it is rapidly transferred to the S_1 state by nonadiabatic transition with a transient lifetime of 7 fs, and (iii) the IVR is initiated in the S_1 state in about 80 fs after optical excitation. The experimentally measured S_2 lifetime of 22 ± 3 fs can be interpreted as related to the overall rate of these processes, which were probably insufficiently time-resolved with a 22 fs resolution.¹³

The present study raised a possibility that the nonradiative transition pathway of pyrazine may be composed of the processes much faster than previously believed. In our WP analysis, the Franck-Condon WP on the PES of the optically bright S_2 state, which is independent of the incident laser pulse, was set as the initial condition. Therefore, the calculated transient lifetime of 7 fs is intrinsic to the nonadiabatic transition via the $S_2 - S_1$ CI. For definite identification of such ultrafast nonradiative processes, time-resolved spectroscopy with an improved temporal resolution of several fs or shorter is highly needed.

Acknowledgements

M. K. is grateful to Dr. W. C. Chung, Dr. Y.-I. Suzuki, and Prof. T. Suzuki for valuable discussions.

This work was supported in part by JSPS KAKENHI Grant Number 26810002.

References

- 1 K. K. Innes, I. G. Ross and W. R. Moomaw, *J. Mol. Spectrosc.*, 1988, **132**, 492.
- 2 W. Domcke, D. R. Yarkony and H. Köppel, *Conical Intersections*, World Scientific, Singapore,

- 2004.
- 3 T. Suzuki and Y.-I. Suzuki, in *Advances in Multi-Photon Processes and Spectroscopy*, ed. S. H. Lin, A. A. Villaeys and Y. Fujimura, World Scientific, Singapore, 2014, vol. 21, ch. 4, pp. 139-174.
- 4 I. Suzuka, Y. Udagawa and M. Ito, *Chem. Phys. Lett.*, 1979, **64**, 333.
- 5 Y. Udagawa, M. Ito and I. Suzuka, *Chem. Phys.*, 1980, **46**, 237.
- 6 I. Yamazaki, T. Murao, T. Yamanaka and K. Yoshihara, *Faraday Discuss. Chem. Soc.*, 1983, **75**, 395.
- 7 J. Kommandeur, W. A. Majewski, W. L. Meerts and D. W. Pratt, *Ann. Rev. Phys. Chem.*, 1987, **38**, 433.
- 8 M. Sukharev and T. Seideman, *Phys. Rev. Lett.*, 2004, **93**, 093004.
- 9 P. S. Christopher, M. Shapiro and P. Brumer, *J. Chem. Phys.*, 2006, **125**, 124310.
- 10 Z. Hu, S. Singha, Y. Zhao, G. E. Barry, T. Seideman and R. J. Gordon, *J. Phys. Chem. Lett.*, 2012, **3**, 2744.
- 11 M. Sala, M. Saab, B. Lasorne, F. Gatti and S. Guérin, *J. Chem. Phys.*, 2014, **140**, 194309.
- 12 V. Stert, P. Farmanara and W. Radloff, *J. Chem. Phys.*, 2000, **112**, 4460.
- 13 Y.-I. Suzuki, T. Fuji, T. Horio and T. Suzuki, *J. Chem. Phys.* **132**, 174302.
- 14 R. Schneider and W. Domcke, *Chem. Phys. Lett.*, 1988, **150**, 235.
- 15 R. Schneider and W. Domcke, *Chem. Phys. Lett.*, 1989, **159**, 61.
- 16 G. Stock, R. Schneider and W. Domcke, *J. Chem. Phys.*, 1989, **90**, 7184.

- 17 R. Schneider, W. Domcke and H. Köppel, *J. Chem. Phys.*, 1990, **92**, 1045.
- 18 G. Stock and W. Domcke, *J. Chem. Phys.*, 1990, **93**, 5496.
- 19 M. Seel and W. Domcke, *J. Chem. Phys.*, 1991, **95**, 7806.
- 20 L. Seidner, G. Stock, A. L. Sobolewski and W. Domcke, *J. Chem. Phys.*, 1992, **96**, 5298.
- 21 C. Woywod, W. Domcke, A. L. Sobolewski and H.-J. Werner, *J. Chem. Phys.*, 1994, **100**, 1400.
- 22 G. Stock, C. Woywod, W. Domcke, T. Swinney and B. S. Hudson, *J. Chem. Phys.*, 1995, **103**, 6851.
- 23 G. A. Worth, H.-D. Meyer and L. S. Cederbaum, *J. Chem. Phys.*, 1996, **105**, 4412.
- 24 G. A. Worth, H.-D. Meyer and L. S. Cederbaum, *J. Chem. Phys.*, 1998, **109**, 3518.
- 25 A. Raab, G. A. Worth, H.-D. Meyer and L. S. Cederbaum, *J. Chem. Phys.*, 1999, **110**, 936.
- 26 G. A. Worth, H.-D. Meyer and L. S. Cederbaum, *Chem. Phys. Lett.*, 1999, **299**, 451.
- 27 P. Puzari, B. Sarker and S. Adhikari, *J. Chem. Phys.*, 2006, **125**, 194316.
- 28 R. X. He, C. Y. Zhu, C.-H. Chin and S. H. Lin, *Chem. Phys. Lett.*, 2009, **476**, 19.
- 29 C.-K. Lin, Y. Niu, C. Zhu, Z. Shuai and S. H. Lin, *Chem. Asian J.*, 2011, **6**, 2977.
- 30 U. Werner, R. Mitrić, T. Suzuki and V. Bonačić-Koutecký, *Chem. Phys.*, 2008, **349**, 319.
- 31 M. Sala, B. Lasorne, F. Gatti and S. Guérin, *Phys. Chem. Chem. Phys.*, 2014, **16**, 15957.
- 32 G. Tomasello, A. Humeniuk and R. Mitrić, *J. Phys. Chem. A*, 2014, **118**, 8437.
- 33 U. Werner, R. Mitrić and V. Bonačić-Koutecký, *J. Chem. Phys.*, 2010, **132**, 174301.
- 34 W. R. Wadt and W. A. Goddard, III, *J. Am. Chem. Soc.*, 1975, **97**, 2034.
- 35 I. C. Walker and M. H. Palmer, *Chem. Phys.*, 1991, **153**, 169.

- 36 Y. Okuzawa, M. Fujii and M. Ito, *Chem. Phys. Lett.*, 1990, **171**, 341.
- 37 J. C. Tully, *J. Chem. Phys.*, 1990, **93**, 1061.
- 38 W. C. Chung, Z. Lan, Y. Ohtsuki, N. Shimakura, W. Domecke and Y. Fujimura, *Phys. Chem. Chem. Phys.*, 2007, **9**, 2075.
- 39 W. M. I. Hassan, W. C. Chung, N. Shimakura, S. Koseki, H. Kono and Y. Fujimura, *Phys. Chem. Chem. Phys.*, 2010, **12**, 5317.
- 40 I. N. Levine, *Quantum Chemistry*, Prentice Hall, New Jersey, 6th edn., 2009, pp. 471-635.
- 41 H.-J. Werner, P. J. Knowles, G. Knizia, F. R. Manby and M. Schütz, *WIREs Comput. Mol. Sci.*, 2012, **2**, 242.
- 42 H.-J. Werner, P. J. Knowles, G. Knizia, F. R. Manby, M. Schütz, P. Celani, T. Korona, R. Lindh, A. Mitrushenkov, G. Rauhut, K. R. Shamasundar, T. B. Adler, R. D. Amos, A. Bernhardsson, A. Berning, D. L. Cooper, M. J. O. Deegan, A. J. Dobbyn, F. Eckert, E. Goll, C. Hampel, A. Hesselmann, G. Hetzer, T. Hrenar, G. Jansen, C. Köppl, Y. Liu, A. W. Lloyd, R. A. Mata, A. J. May, S. J. McNicholas, W. Meyer, M. E. Mura, A. Nicklass, D. P. O'Neill, P. Palmieri, D. Peng, K. Pflüger, R. Pitzer, M. Reiher, T. Shiozaki, H. Stoll, A. J. Stone, R. Tarroni, T. Thorsteinsson and M. Wang, MOLPRO, version 2012.1, Cardiff, UK, 2012.
- 43 H.-J. Werner and P. J. Knowles, *J. Chem. Phys.*, 1985, **82**, 5053.
- 44 P. J. Knowles and H.-J. Werner, *Chem. Phys. Lett.*, 1985, **115**, 259.
- 45 H.-J. Werner and P. J. Knowles, *J. Chem. Phys.*, 1988, **89**, 5803.
- 46 P. J. Knowles and H.-J. Werner, *Chem. Phys. Lett.*, 1988, **145**, 514.

- 47 P. J. Knowles and H.-J. Werner, *Theor. Chim. Acta*, 1992, **84**, 95.
- 48 D. R. Yarkony, *Rev. Mod. Phys.*, 1996, **68**, 985.
- 49 D. R. Yarkony, *Acc. Chem. Res.*, 1998, **31**, 511.
- 50 D. R. Yarkony, *Chem. Rev.*, 2012, **112**, 481.
- 51 M. Kanno, H. Kono, Y. Fujimura and S. H. Lin, *Phys. Rev. Lett.*, 2010, **104**, 108302.
- 52 M. Kanno, H. Kono and Y. Fujimura, in *Progress in Ultrafast Intense Laser Science*, ed. K. Yamanouchi, D. Charalambidis and D. Normand, Springer, Berlin, 2011, vol. 7, ch. 3, pp. 53-78.
- 53 M. Kanno, H. Kono, S. H. Lin and Y. Fujimura, in *Quantum Systems in Chemistry and Physics: Progress in Methods and Applications*, ed. K. Nishikawa, J. Maruani, E. J. Brändas, G. Delgado-Barrio and P. Piecuch, Springer, Netherlands, 2012, Progress in Theoretical Chemistry and Physics vol. 26, ch. 6, pp. 121-148.
- 54 M. Kanno, Y. Ono, H. Kono and Y. Fujimura, *J. Phys. Chem. A*, 2012, **116**, 11260.
- 55 M. Kanno, Y. Ono, H. Kono and Y. Fujimura, *Chin. J. Phys.*, 2014, **52**, 617.
- 56 M. Baer, *Beyond Born-Oppenheimer*, Wiley, Hoboken, New Jersey, 2006, ch. 2, pp. 26-57.
- 57 B. Sarkar and S. Adhikari, *Int. J. Quant. Chem.*, 2009, **109**, 650.
- 58 D. Simah, B. Hartke and H.-J. Werner, *J. Chem. Phys.*, 1999, **111**, 4523.
- 59 Y. Ohtsuki, K. Nakagami and Y. Fujimura, in *Advances in Multi-Photon Processes and Spectroscopy*, ed. S. H. Lin, A. A. Villaeys and Y. Fujimura, World Scientific, Singapore, 2001, vol. 13, ch. 1, pp. 1-127.

- 60 P. Gross, D. Neuhauser and H. Rabitz, *J. Chem. Phys.*, 1992, **96**, 2834.
- 61 S. Craddock, P. B. Liescheski, D. W. H. Rankin and H. E. Robertson, *J. Am. Chem. Soc.*, 1988, **110**, 2758.
- 62 P. Weber and J. R. Reimers, *J. Phys. Chem. A*, 1999, **103**, 9821.
- 63 The TDDFT vertical excitation energy to the S₄ state given in ref. 30 is 6.3 eV; however, our calculation at the same B3LYP/TZVP level of theory yielded 5.60 eV for the S₄ state and 6.35 eV for the S₅ (¹B_{1g}) state. Lin *et al.* reported 5.57 eV for the S₄ state, which is almost equal to our value, calculated at the B3LYP/6-311++G** level of theory in ref. 29.
- 64 M. J. Frisch, G. W. Trucks, H. B. Schlegel, G. E. Scuseria, M. A. Robb, J. R. Cheeseman, G. Scalmani, V. Barone, B. Mennucci, G. A. Petersson, H. Nakatsuji, M. Caricato, X. Li, H. P. Hratchian, A. F. Izmaylov, J. Bloino, G. Zheng, J. L. Sonnenberg, M. Hada, M. Ehara, K. Toyota, R. Fukuda, J. Hasegawa, M. Ishida, T. Nakajima, Y. Honda, O. Kitao, H. Nakai, T. Vreven, J. A. Montgomery, Jr., J. E. Peralta, F. Ogliaro, M. Bearpark, J. J. Heyd, E. Brothers, K. N. Kudin, V. N. Staroverov, R. Kobayashi, J. Normand, K. Raghavachari, A. Rendell, J. C. Burant, S. S. Iyengar, J. Tomasi, M. Cossi, N. Rega, J. M. Millam, M. Klene, J. E. Knox, J. B. Cross, V. Bakken, C. Adamo, J. Jaramillo, R. Gomperts, R. E. Stratmann, O. Yazyev, A. J. Austin, R. Cammi, C. Pomelli, J. W. Ochterski, R. L. Martin, K. Morokuma, V. G. Zakrzewski, G. A. Voth, P. Salvador, J. J. Dannenberg, S. Dapprich, A. D. Daniels, O. Farkas, J. B. Foresman, J. V. Ortiz, J. Cioslowski and D. J. Fox, Gaussian 09, revision A.02, Gaussian, Inc., Wallingford CT, 2009.
- 65 M. V. Berry, *Proc. R. Soc. A*, 1984, **392**, 45.

Table 1 Experimental and calculated geometrical parameters at the D_{2h} equilibrium geometry in the S_0 state of pyrazine. Bond lengths and angles are in Å and degrees, respectively.

| | Exp. ^a | CASSCF |
|------|-------------------|--------|
| CH | 1.083 | 1.075 |
| CN | 1.338 | 1.330 |
| CC | 1.397 | 1.395 |
| ∠CNC | 115.7 | 116.0 |
| ∠CCH | 120.0 | 120.7 |

^a From gas-phase electron diffraction and liquid-crystal NMR.⁶¹

Table 2 Experimental and calculated harmonic vibrational frequencies of the Q_{6a} , Q_{10a} , Q_4 , and Q_5 normal modes at the D_{2h} equilibrium geometry in the S_0 state of pyrazine in units of cm^{-1} .

| Symmetry | Mode | Exp. ^a | CASSCF |
|----------|-----------|-------------------|--------|
| a_g | Q_{6a} | 596 | 643 |
| b_{1g} | Q_{10a} | 919 | 962 |
| b_{2g} | Q_4 | 756 | 782 |
| | Q_5 | 983 | 999 |

^a From IR and Raman spectroscopies.¹

Table 3 Experimental and calculated vertical excitation energies to the lowest four singlet excited states at the D_{2h} equilibrium geometry in the S_0 state of pyrazine in units of eV. The MRCISD energies were obtained by a single-point calculation at the CASSCF optimized geometry.

| State | Exp. | TDDFT ^e | CASSCF | XMCQDPT2 ^f | MRCISD |
|----------------------------------|-------------------|--------------------|--------|-----------------------|--------|
| S_4 (${}^1B_{2g}, n\pi^*$) | 5.19 ^a | 5.60 ⁶³ | 5.92 | 5.38 | 5.91 |
| S_3 (${}^1A_u, n\pi^*$) | 5.0 ^b | 4.61 | 6.03 | 4.45 | 5.52 |
| S_2 (${}^1B_{2u}, \pi\pi^*$) | 4.81 ^c | 5.46 | 5.02 | 4.79 | 5.16 |
| S_1 (${}^1B_{3u}, n\pi^*$) | 3.97 ^d | 3.96 | 4.76 | 3.93 | 4.55 |

^a From UV-IR fluorescence dip spectroscopy.³⁶

^b From near-threshold electron energy-loss spectroscopy.³⁵

^c From UV absorption.¹

^d Estimated as the sum of adiabatic excitation and average reorganization energies.⁶²

^e With the B3LYP functional and the TZVP basis set.³⁰

^f Based on the CASSCF reference with the aug-cc-pVDZ basis set and the same active space as in the present calculations.³¹

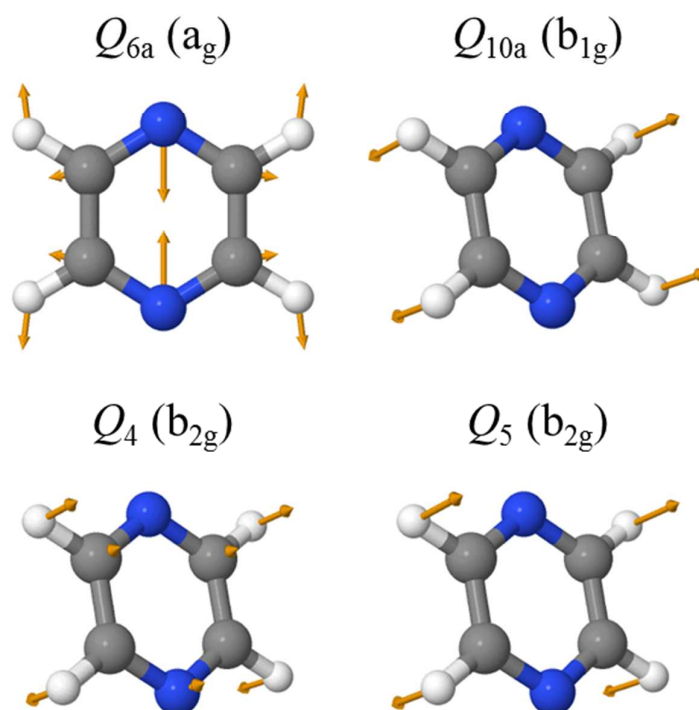


Fig. 1 D_{2h} optimized geometry and selected normal modes in the S_0 state of pyrazine. The irreducible representations to which each mode belongs are given in parentheses. The white, black, and blue balls represent hydrogen, carbon, and nitrogen atoms, respectively. The arrows indicate the directions of the vibrational vectors of the normal modes.

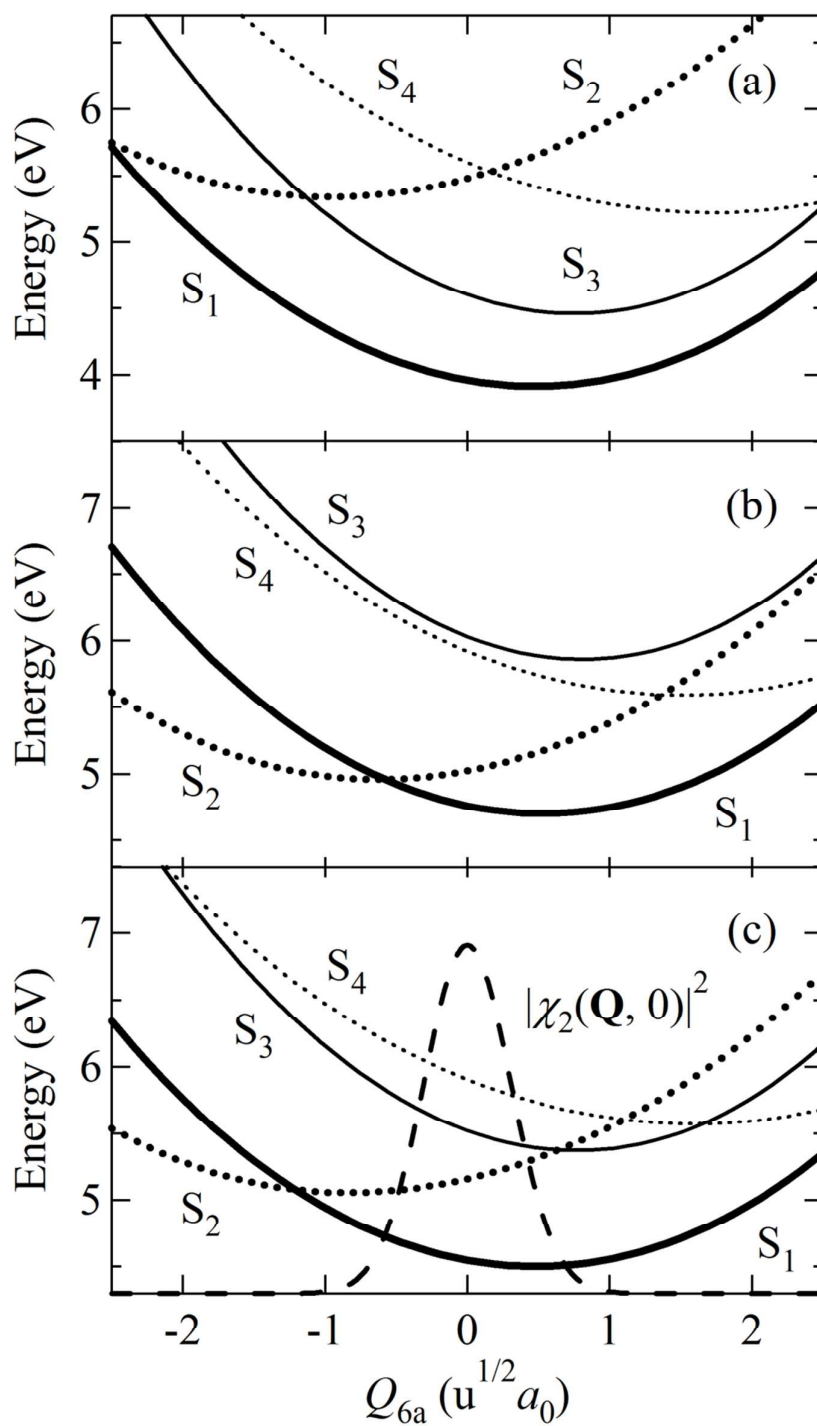


Fig. 2 One-dimensional (a) TDDFT, (b) CASSCF, and (c) MRCISD PESs of the lowest four singlet excited states along the tuning mode Q_{6a} . The bold solid, bold dotted, thin solid, and thin dotted lines denote the PESs of the S_1 (${}^1B_{3u}$), S_2 (${}^1B_{2u}$), S_3 (1A_u), and S_4 (${}^1B_{2g}$) states, respectively.

The broken line in panel (c) represents the probability density of the Franck-Condon WP along the Q_{6a} mode in arbitrary units.

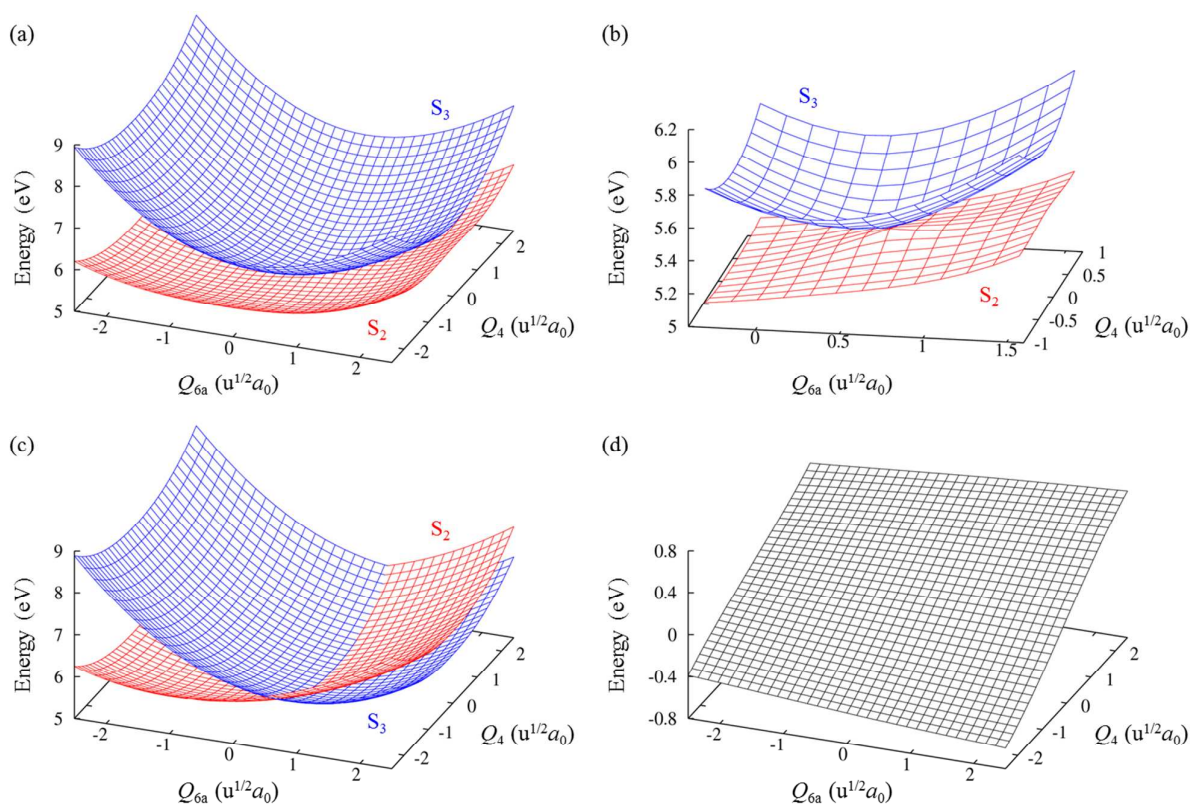


Fig. 3 (a) MRCISD adiabatic PESs of two 1A_u states, S_2 and S_3 , in the $Q_{6a} - Q_4$ subspace. (b) Close-up view of the $S_3 - S_2$ CI. (c) MRCISD diabatic PESs of the two excited states and (d) their diabatic coupling.

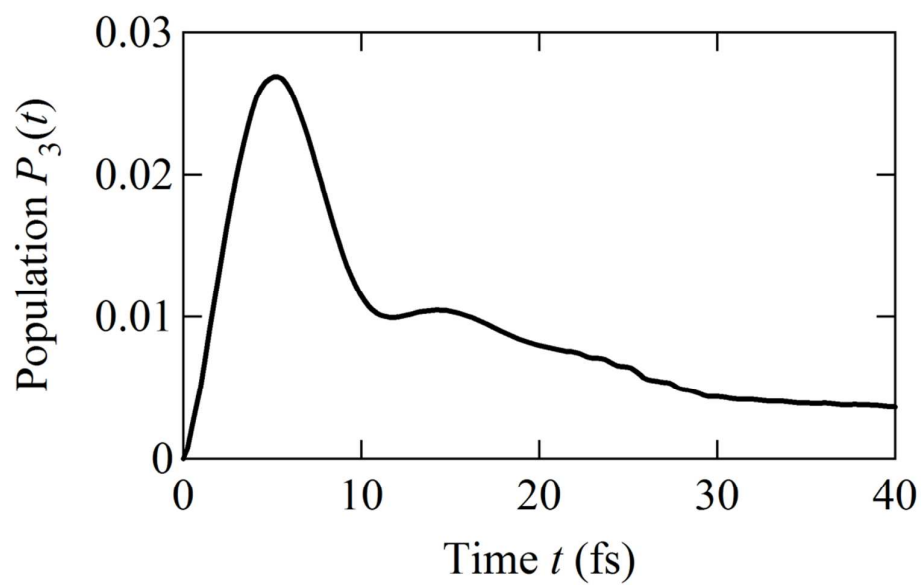


Fig. 4 Temporal behavior in the population of the S_3 state, $P_3(t)$, in the $Q_{6a} - Q_4$ subspace.

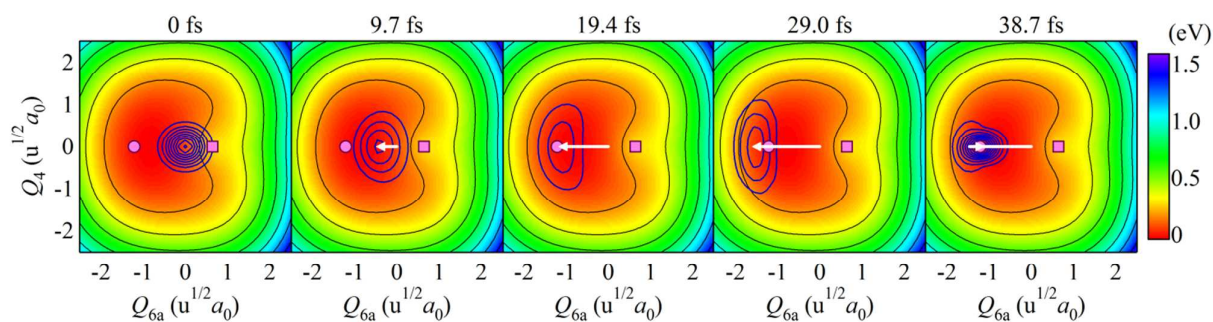


Fig. 5 Snapshots of the adiabatic WP on the S_2 PES in the $Q_{6a} - Q_4$ subspace. The zero of potential energy is set to the minimum of the PES. The bold contours represent the probability density $|\chi_2(\mathbf{Q}, t)|^2$ and the arrows indicate the trajectory of the expectation value of the normal coordinate \mathbf{Q} of the WP, $\mathbf{Q}_2(t)$. The positions of the $S_3 - S_2$ and $S_2 - S_1$ CIs are signified by a square and circle, respectively.

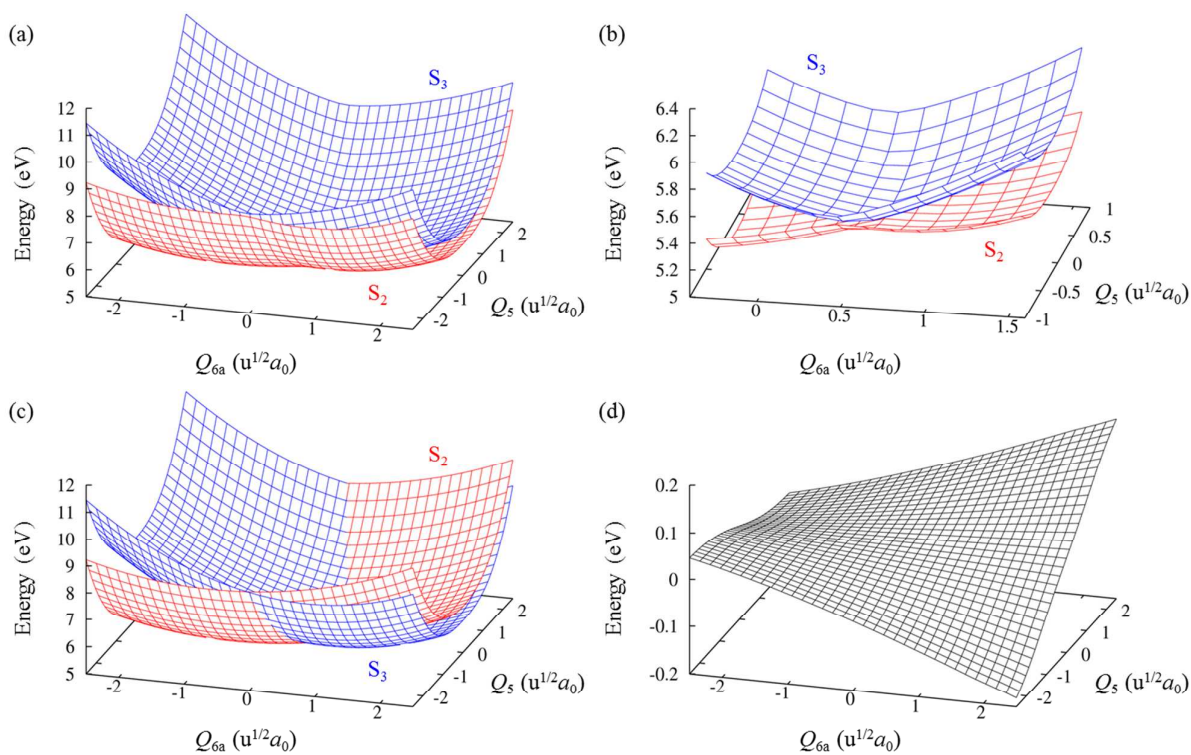


Fig. 6 (a) MRCISD adiabatic PESs of two 1A_u states, S_2 and S_3 , in the $Q_{6a} - Q_5$ subspace. (b) Close-up view of the $S_3 - S_2$ CI. (c) MRCISD diabatic PESs of the two excited states and (d) their diabatic coupling.

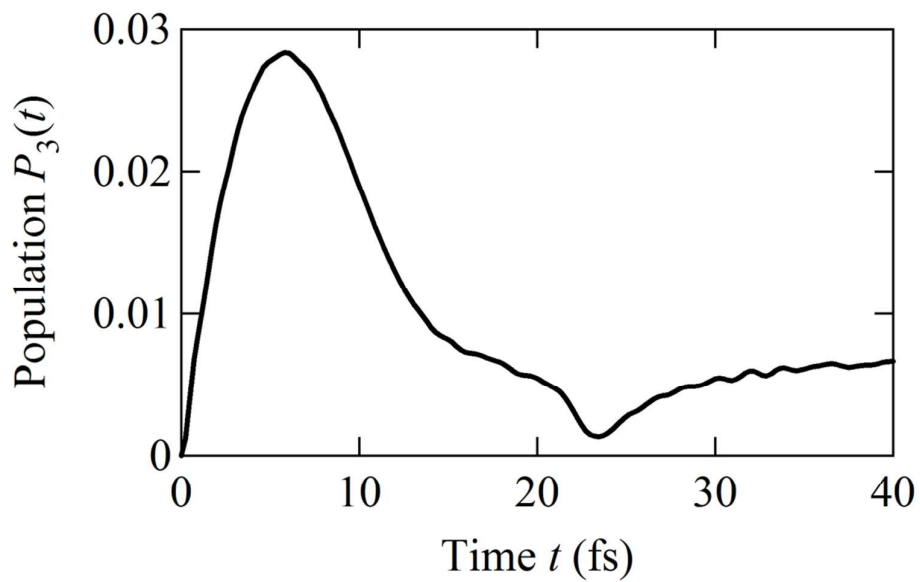


Fig. 7 Temporal behavior in the population of the S_3 state, $P_3(t)$, in the $Q_{6a} - Q_5$ subspace.

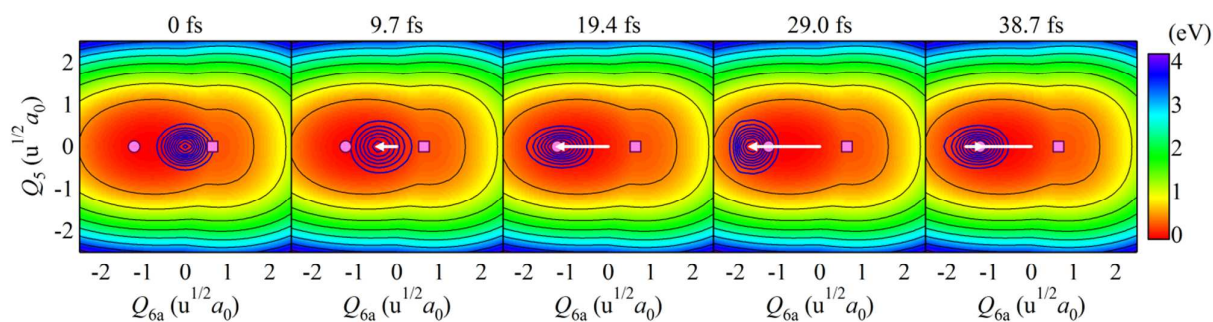


Fig. 8 Snapshots of the adiabatic WP on the S_2 PES in the $Q_{6a} - Q_5$ subspace. The zero of potential energy is set to the minimum of the PES. The bold contours represent the probability density $|\chi_2(\mathbf{Q}, t)|^2$ and the arrows indicate the trajectory of the expectation value of the normal coordinate \mathbf{Q} of the WP, $\mathbf{Q}_2(t)$. The positions of the $S_3 - S_2$ and $S_2 - S_1$ CIs are signified by a square and circle, respectively.

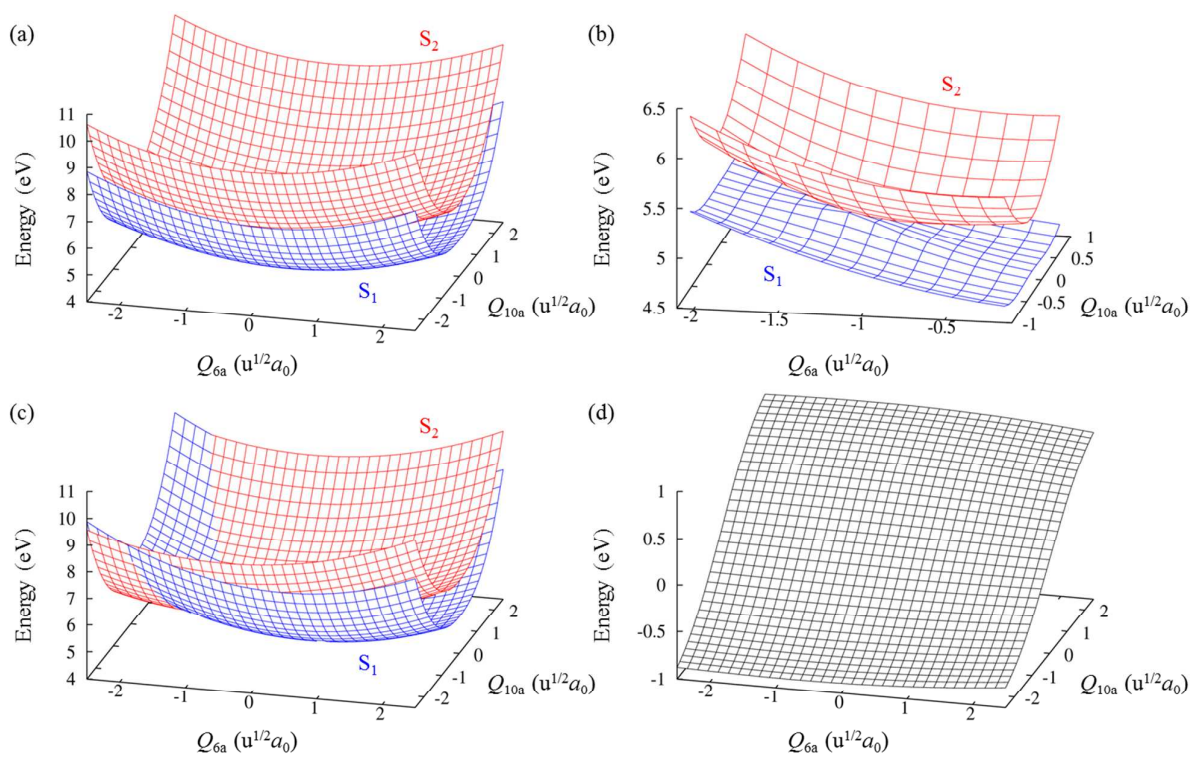


Fig. 9 (a) MRCISD adiabatic PESs of two 1B_u states, S_1 and S_2 , in the $Q_{6a} - Q_{10a}$ subspace. (b) Close-up view of the $S_2 - S_1$ CI. (c) MRCISD diabatic PESs of the two excited states and (d) their diabatic coupling.

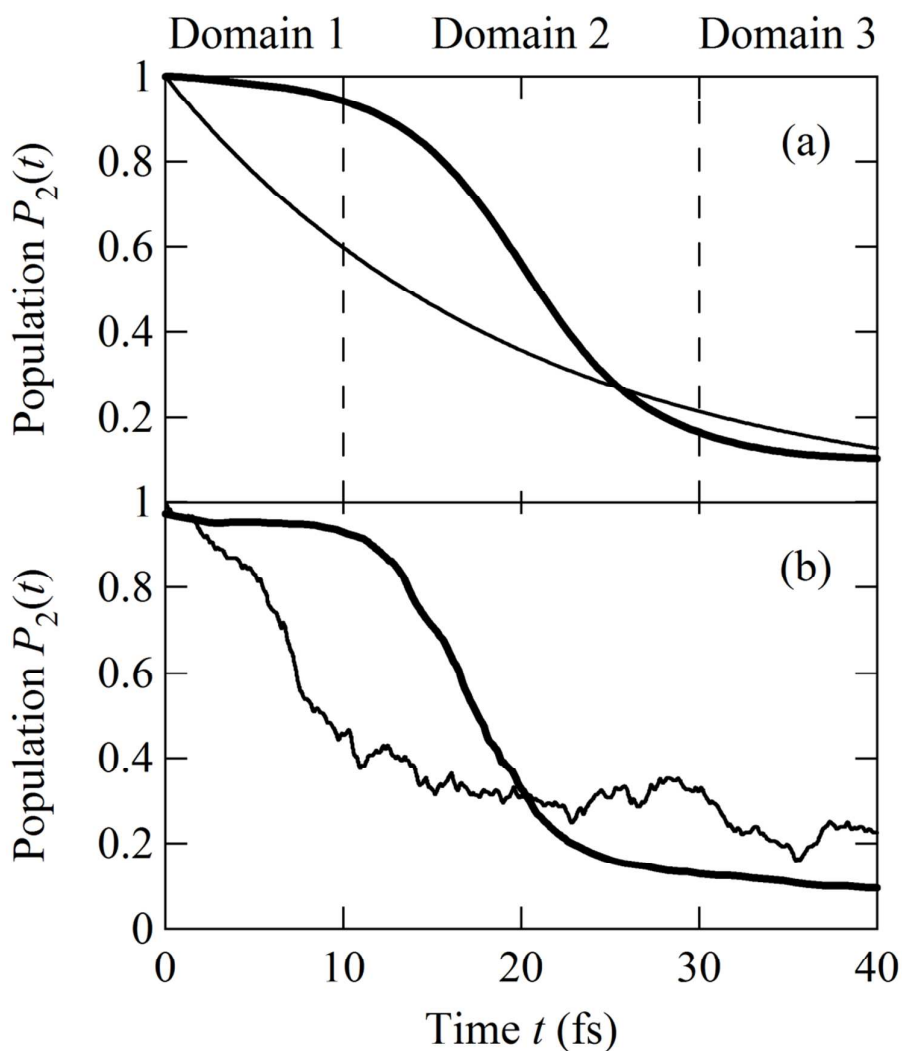


Fig. 10 (a) Temporal behavior in the population of the S_2 state, $P_2(t)$, in the $Q_{6a} - Q_{10a}$ subspace (bold solid line) and its exponential decay fit with a lifetime of 19.4 fs (thin solid line). The vertical broken lines indicate the crude boundaries between the three time domains of nonradiative transition at $t = 10$ and 30 fs. (b) The S_2 populations obtained in the TDDVR calculation with a 24-mode model Hamiltonian²⁷ (bold solid line) and the on-the-fly surface hopping calculation combined with the TDDFT³⁰ (thin solid line).

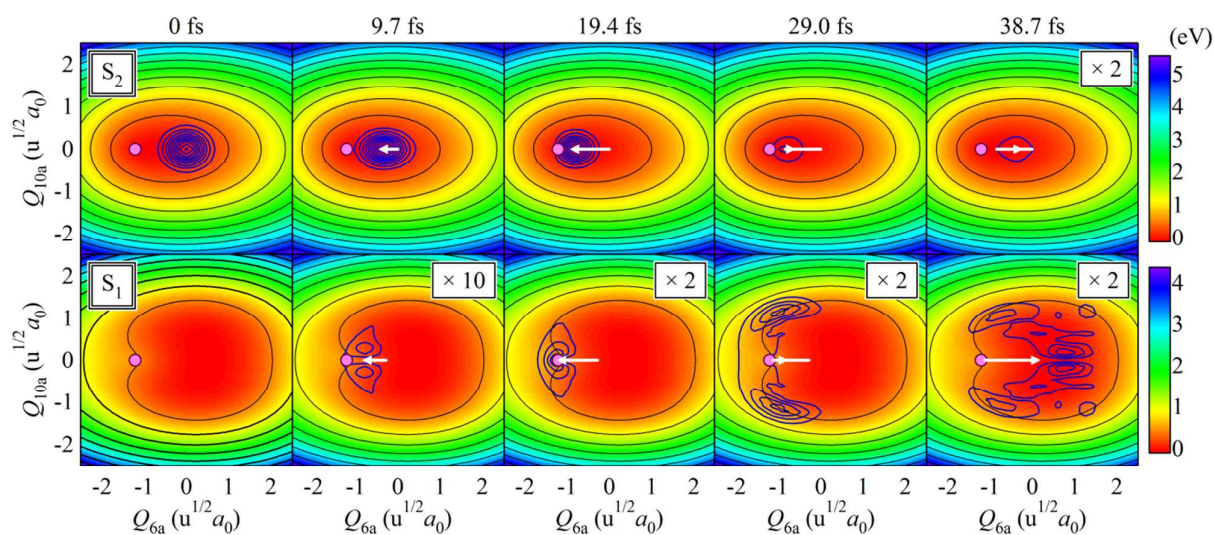


Fig. 11 Snapshots of the adiabatic WPs on the S_2 (top panels) and S_1 (bottom panels) PESs in the $Q_{6a} - Q_{10a}$ subspace. The zero of potential energy is set to the minimum of each PES. The bold contours represent the probability densities $|\chi_2(\mathbf{Q}, t)|^2$ and $|\chi_1(\mathbf{Q}, t)|^2$ and the arrows indicate the trajectory of the expectation value of the normal coordinate \mathbf{Q} of each WP, $\mathbf{Q}_2(t)$ and $\mathbf{Q}_1(t)$. The position of the $S_2 - S_1$ CI is signified by a circle.

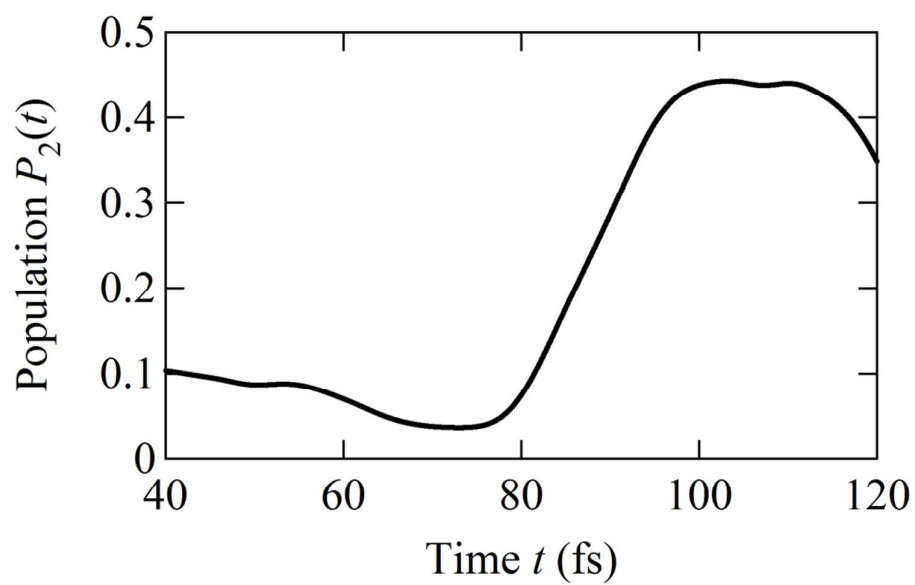


Fig. 12 Temporal behavior in the population of the S_2 state, $P_2(t)$, in the $Q_{6a} - Q_{10a}$ subspace at $t > 40$ fs.

Table of contents entry

Ab initio quantum dynamical calculations reveal the contributions of the optically dark S_1 ($^1B_{3u}$), S_3 (1A_u), and S_4 ($^1B_{2g}$) states to ultrafast nonradiative transition from the optically bright S_2 ($^1B_{2u}$) state in pyrazine and suggest a much faster transition rate than previously believed.

